Earth and Space Science

RESEARCH ARTICLE
10.1029/2020EA001286

Special Section:
InSight at Mars

Finding SEIS North on Mars: Comparisons Between SEIS Sundial, Inertial and Imaging Measurements and Consequences for Seismic Analysis

D. Savoie[1,2], A. Richard[2], M. Goutaudier[2], P. Lognonné[3], K. J. Hurst[4], J. N. Maki[4], M. P. Golombek[4], M. van Driel[5], J. Clinton[6], E. Stutzmann[3], D. Mimoun[7], W. B. Banerdt[4], and N. R. Williams[4]

[1]SYRTE, Observatoire de Paris, Université PSL, CNRS, Sorbonne Université, Paris, France, [2]Palais de La Découverte, Paris, France, [3]Université de Paris, Institut de physique du globe de Paris, CNRS, Paris, France, [4]NASA Jet Propulsion Laboratory, California Institute of Technology, Pasadena, CA, USA, [5]Institute of Geophysics, ETH Zurich, Zurich, Switzerland, [6]Swiss Seismological Service, ETH Zurich, Zurich, Switzerland, [7]Institut Supérieur de L'Aéronautique et de L'Espace, ISAE, Toulouse, France

Key Points:

- True North on Mars has been found using a sundial during the InSight mission
- This reference direction is used for Marsquakes location

Correspondence to:
D. Savoie, A. Richard, and M. Goutaudier,
denis.savoie@obspm.fr;
andy.richard@universcience.fr;
marc.goutaudier@universcience.fr

Citation:
Savoie, D., Richard, A., Goutaudier, M., Lognonné, P., Hurst, K. J., Maki, J. N., et al. (2021). Finding SEIS North on Mars: Comparisons between SEIS sundial, Inertial and Imaging measurements and consequences for seismic analysis. *Earth and Space Science*, *8*, e2020EA001286. https://doi.org/10.1029/2020EA001286

Received 3 JUN 2020
Accepted 12 JAN 2021

Abstract In this paper, we present the results obtained in the determination of the true north direction on Mars by using a gnomon on the InSight mission and compare the measurements with either the North determination from the Inertial Measurement Unit and imaging analysis. The obtained measurement has been used to populate the SEIS orientation information in the archived SEIS data. Images taken during December 2018 and January 2019 allow to determine the gnomon shadow position and length over a target. By calculating the Sun local coordinates using planetary ephemeris VSOP87, the images are used to estimate the true North direction on the landing site. By using eight different images selected, we obtain the true North direction with an accuracy up to 2.5°, which is confirmed by the IMU and imaging analysis. The true North direction is also confirmed by an image taken near local noon, when the sun crosses the meridian. The North determination precision is then discussed in view of the seismic determination of the back azimuth.

1. Introduction

NASA's InSight landing on Mars took place on November 26, 2018. After a few weeks of surface operations, InSight deployed the seismometer package SEIS (Seismic Experience for Interior Structure, Lognonné et al., 2019) on the martian surface and provided first results (Banerdt et al., 2020; Giardini et al., 2020; Lognonné et al., 2020). Many of the SEIS scientific investigations were made by the three axis capability of the SEIS instrument, enabling the measurement, in the North, East, vertical local reference, of the ground acceleration. This paper is therefore focused on the methods used to determine this reference frame. While SEIS has its vertical axis, thanks to its leveling system, aligned with the local gravity to within less than 0.1°, the determination of its azimuth with respect to true North, i.e. direction toward the geographic North pole, was more difficult.

The top of the instrument is equipped with a handle used during deployment that also doubles as a gnomon. A gnomon is the main tool of a sundial: a vertical stick projecting a shadow on a target. It enables, by its shadow, the determination of the position of the Sun in the sky, and thus by extension in our case the seismometer position and orientation on the Martian surface.

As an example, most of the instruments installed on the Moon by Apollo missions as part of the Apollo Lunar Surface Experiments Package (ALSEP, see Sullivan, 1994), be it passive seismometers, laser reflectors (still used for Lunar laser ranging), the analyzer of ejecta and meteorites, etc., were all oriented with the help of a gnomon whose shadow was projected on a target (Figure 1). In this case however, it is better to speak of "solar compass". Orientation on the Moon by the azimuth of the Sun was indeed extremely easy due to the very slow variation of this angle, which remains almost constant for several hours.

For InSight too, the technique did not require any active sensor, as it used in an opportunistic way the InSight camera (Maki et al., 2018) and the deployment handle. This was simpler than the north sensor of the Small Surface Stations of Mars 96 (Linkin et al., 1998, unfortunately lost after launch in 11/1996), which

Figure 1. Gnomon used on the Moon with the passive seismic experiment (PSE) during the Apollo 14 mission.

had also to determine the North for the magnetic components of the OPTIMISM experiment (Kuhnke et al., 1998; Lognonné et al., 1998). Their North sensor, mounted on the deployed magnetometer, was monitored the light intensity through a small hole with a known direction with respect to the three axis of the magnetometer.

For InSight, the gnomon was only visible for a few days after the deployment of SEIS. The seismometer was subsequently covered by the Wind and Thermal Shield (WTS) before starting its operation phase. The process to determine the true North direction by using a gnomon on Mars was described by Savoie et al. (2019), from which this paper presents the results.

In this paper, we describe the procedures and results obtained during the few days after the SEIS seismometer was deployed on the martian surface, in order to determine the true North using the gnomon. We first describe the method used to analyze the InSight camera images. Determination of the true North requires identification of the whole shadow on low quality images deformed by the perspective. Then, we describe the results obtained for the true North direction on the different images selected.

We then compare the gnomon North determination with an independent measure of the lander azimuth, as obtained from the Inertial Measurement Unit. From that azimuth and the exact knowledge of the Instrument Deployment Arm imager, it was therefore possible to determine also the direction of North with respect to SEIS. A second comparison is then done through the analysis of remote sensing data and their comparison with the lander panorama images.

We conclude the paper by comparing the orientation errors with the determination of the back azimuth of seismic signals, which is the azimuth of the seismic rays when they reach the station. This measurement provides the direction of the source from InSight's location. We then confirm that the North orientation is meeting all the seismological needs. The SEIS orientation presented in this paper has therefore been used as reference, and is included in the SEIS metadata (InSight Mars SEIS Data Service, 2019).

2. Images Taken by the Instrument Deployment Camera (IDC)

After landing, images of the SEIS sundial were acquired by the Instrument Deployment Camera located on the robotic arm as described by Maki et al. (2018). The IDC has an angular resolution of approximately 0.82 milli-radians/pixel at the center of the image and a field of view of 45° (horizontal) × 45° (vertical). After the deployment of SEIS on the surface on 19 December 2018, IDC images of the sundial were acquired from approximately 1 meter above the sundial.

2.1. Image Sources

The images are published on the InSight mission website (https://mars.nasa.gov/insight/multimedia/raw-images) and labeled with date and local mean solar time (LMST). The first images with a clearly visible shadow were taken on January 1st, 2019. To determine the true North direction, we selected eight images acquired on January 1st, 2019, and labeled from 12 h 49 m 37 s to 15 h 42 m 05 s LMST (see for example Figure 2).

Due to a very tight schedule for the InSight ground operations, these images were taken within a few minute range, thus having very similar shadow positions and lengths. As explained by Savoie et al. (2019), this configuration is not ideal to reach the accuracy of 1° in true North direction but it allows us to reach the expected accuracy of 5° nonetheless.

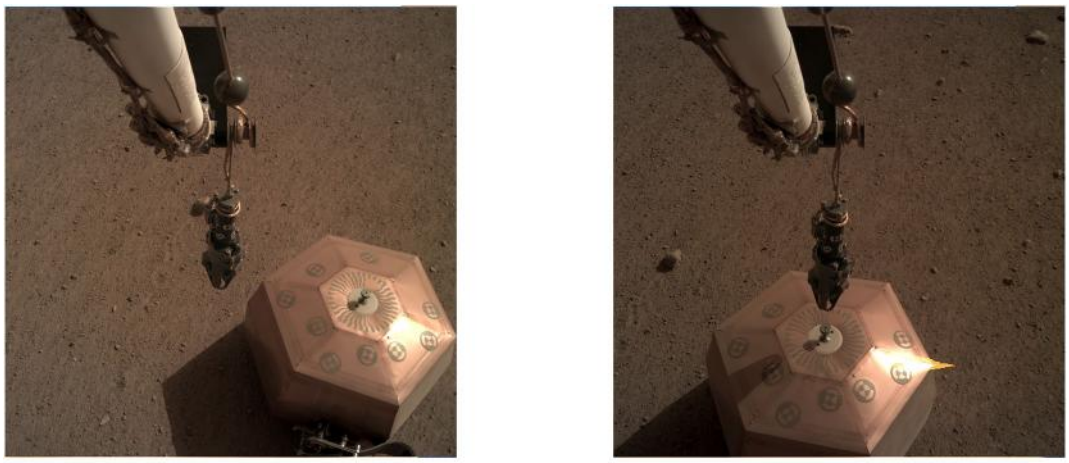

(a) 01/01/19 - 15h08m25s LMST (b) 01/01/19 - 15h37m32s LMST

Figure 2. Images of the sundial taken on January 1st, 2019. The gnomon shadow is visible on the target that is used to measure the azimuth of the Sun.

Furthermore, the image taken near local noon can be used as a confirmation of the true North direction estimation, the Sun being close to the meridian. On this particular image however, the Sun is passing high in the sky and the gnomon shadow is too short to reach the target on the sundial. Its direction can still be used to confirm the results obtained with images taken in the afternoon.

In this study, we neglected the nonhorizontality of the sundial which was measured as below 0.1° after the deployment phase of SEIS.

2.2. Determination of the Time

The images file names contain the spacecraft clock time given in seconds elapsed since J2000 (see Figure 3). This timing is given by the free-running onboard clock, and is thus not synchronized with UTC since the spacecraft launch. Since May 2018, the onboard clock has regularly drifted, and continued to do so after landing as seen on Figure 4. This drift is caused by an expected error in the crystal oscillator frequency of the onboard clock. The conversion from spacecraft time to UTC can be made by using the WebGeocalc algorithm (https://wgc.jpl.nasa.gov:8443/webgeocalc/#TimeConversion). For example, the first image taken on January 1st, 2019 (Sol 35) contain a timestamp of 599,635,689 s after J2000. This timestamp corresponds to

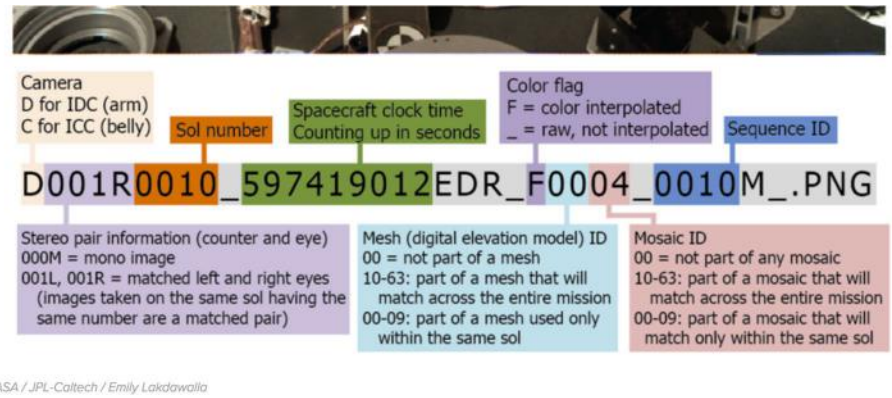

Figure 3. Description of the information contained in the image file name.

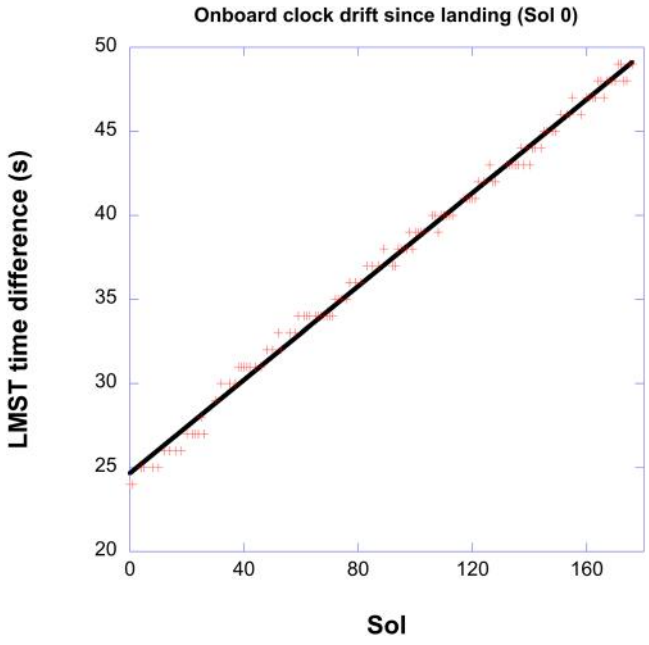

Figure 4. Drift in the Local Mean Solar Time due to the free-running onboard clock on InSight spacecraft. Here, the LMST time difference corresponds to the difference between the onboard time converted using WebGeocalc algorithm and Savoie et al. (2019) algorithm, expressed as integers. The data are plotted for 6 months from Sol 0 (November 26th, 2018). The dark line is fitted to the data, and corresponds to a linear increase of the drift of 0.139 s per sol.

January 1st, 2019 at 17 h 28 m 38 s UTC. By using our algorithm (Savoie et al., 2019), this time is converted to 12 h 49 m 37 s LMST at the InSight landing site.

It is important to notice that this local mean solar time value is different from the one published on the JPL website. For this particular image, the description reads 12 h 51 m 02 s LMST, thus a time difference of 85 s with our calculation.

As detailed by Savoie et al. (2019), a Sun azimuth offset of ± 0°6′, is equivalent to an error of 10 s in timing. A difference of 85 s induces an azimuth error of maximum 54′ for the date of January 1st 2019. This difference induced in the shadow position is below our reading accuracy on the sundial images. This time shift of 85 s can be imputed to the local time conversion algorithm used by JPL which uses prelanding lander coordinates.

The local mean solar time conversion algorithm used by the on the website, implemented in NAIF/SPICE kernels (https://naif.jpl.nasa.gov/pub/naif/INSIGHT/kernels/sclk/insight_lmst_ops181206_v1.tsc) is based on the InSight target landing site coordinates 4.46°N and 135.97°E. However, those coordinates correspond to the prelanding lander coordinates, and are different from the real lander planetocentric coordinates which are 4.50247°N, 135.6,180,843°E (Parker et al., 2019) (Golombek, Williams, et al., 2020).

The main difference between these two sets of coordinates is in the longitude. InSight landed about 0.35° (i.e. 20 km) west-northwest of the planned landing site. Due to Mars rotation, a difference of 0.35° of longitude for the landing site induces a time shift of about 84 s in local mean time.

The coordinates of InSight after landing were updated in the NAIF/SPICE Kernel in April 2019 (https://naif.jpl.nasa.gov/pub/naif/INSIGHT/kernels/fk/insight_tp_ops181206_iau2000_v1.tf), leading to a better agreement with our calculation after this date. This difference does not have an impact on the other scientific activities of the InSight mission, however the sundial is sensitive to any error in position and/or timing.

The reader should also be aware that images taken before December 29th, 2019 are labeled on the JPL website with a wrong local mean solar time value. The value given is actually the local true solar time, which differs from the LMST by almost 50 min.

3. True North Direction on Images

On the sundial, the shadow marks the opposite direction of the Sun. Thus, measuring the shadow position on the sundial at a precise UTC time value provides the Sun azimuth on the pictures. Computing the azimuth of the Sun on Mars allows to determine, on each picture, the location of the North-South axis from which it is measured.

3.1. Possible Errors Committed in the true north determination

Savoie et al. (2019) presents in details the possible errors that can undermine the true North direction determination. These errors can be summarized as:

- Errors due to an incorrect estimation of the shadow position on the images
- Errors due to an incorrect latitude of the lander
- Errors due to an incorrect longitude or UTC value for the lander
- Errors due to gnomon nonverticality

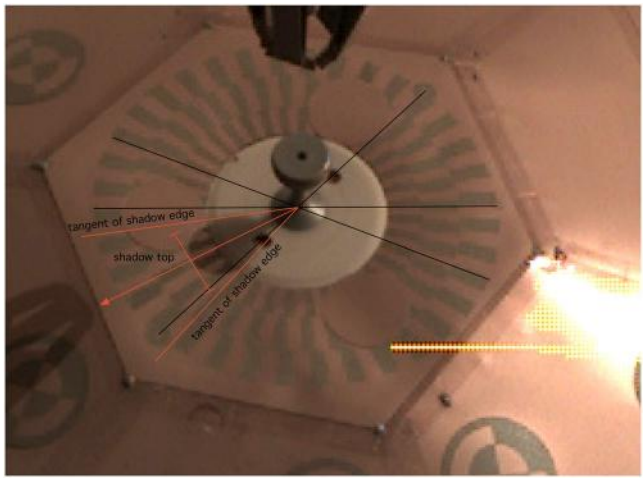

Figure 5. Estimation of the shadow direction on the image taken on 01/01/19 at 15 h 33 m 33 s LMST. Dark rays define the shadow center and red rays define the shadow border, shadow top tangent and shadow top direction.

The main error source is the first. Determination of the exact shadow direction on the images is made difficult by the round-shaped gnomon on top of SEIS and the images quality. The method used to determine shadows directions is detailed in Section 2.2.

After deployment of SEIS, the instrument is leveled with accuracy of 0.1°. Savoie et al. (2019) shows that at this value of horizontality, the maximum error expected on the Sun azimuth is less than 15′ at noon. Since most of the analyzed images are around 15:00 LMST, the error on the hour angle is even less than 5′.

The error due to an incorrect position, either in latitude or longitude is here negligible. A 10 km error on longitude induces a maximum error of 6′ on azimuth. Due to the very precise knowledge of InSight location (discussed in Section 3), the error on azimuth determination due to an incorrect position of the lander is negligible.

Finally, the error in UTC value for images timing detailed in the previous subsection is still negligible on the sundial image.

3.2. Methodology

To determine the true North direction on SEIS images, the following process is applied:

- Find the center of the target at the intersection of diagonals (black lines of Figure 5)
- Graphically estimate the shadow borders on the target (red lines edging the shadow on Figure 5)
- Graphically estimate the center of the shadow line as the bisector of the edges (diagonal red line on Figure 5), and estimate the shadow top tangent
- Compute the Sun azimuth expected for time and location of the image
- Determine the true North direction based on the shadow position as a reference for the Sun azimuth

The quality of images, the distance of the camera and the very large shadow thus induce the biggest error sources of a visual true North determination. Each step of this process is contributes to the global uncertainty. Parts of this process are discussed below.

3.3. Shadow Direction

A precise determination of the shadow top and direction is difficult due to the odd shape and geometry of the gnomon (see Savoie et al., 2019 for a precise description). Due to the gnomon elevation compared to the target level, the center of the whole target has to be determined on each picture.

The target is divided in three concentric rings, each one of them divided into 72 segments of 5° each. The borders of opposite segments can be prolongated through the whole target plane in order to determine the target center.

The defined center can be used to trace rays fitting the round shadow borders. Then, the bisector provides the shadow direction (Figure 5).

3.4. Local Sun Azimuth

The determination of the shadow direction provides the sun direction on the pictures. This direction can be computed by determining azimuth measured in the clockwise direction from the true South. For each picture, we computed the solar coordinates for a Martian observer as described by Savoie et al. (2019). The azimuth and elevation values obtained for the images of January 1st, 2019 are provided in Table 1.

As expected for this local time, the elevation of the Sun is decreasing in the afternoon sky at the InSight landing site. Also, its azimuth is increasing as the Sun is moving toward West ($A = 90°$).

Table 1
Computed Sun Local Coordinates for InSight Images on 01/01/2019

File name	Time			Azimuth	Elevation
(sec since J2000)	UTC	LMST	LTST	A (°)	h (°)
599,635,689	17:28:38	12:49:37	12:00:24	0.2589	68.4926
599,644,246	19:51:15	15:08:25	14:19:11	57.1352	49.4614
599,644,365	19:53:14	15:10:21	14:21:08	57.4756	49.0567
599,645,280	20:08:29	15:25:12	14:35:57	59.8710	45.8976
599,645,795	20:17:04	15:33:33	14:44:18	61.0645	44.0868
599,645,918	20:19:07	15:35:32	14:46:18	61.3348	43.6513
599,646,041	20:21:10	15:37:32	14:48:18	61.5996	43.2146
599,646,321	20:25:50	15:42:05	14:52:50	62.1830	42.2166

3.5. True North Direction Results

On each image, we used the method described earlier to determine the top of the shadow, and thus the Sun, direction. The azimuth of the Sun associated then leads to the North-South axis. The results are given here for two of the eight different images taken on January 1st, 2019 (Figures 6 and 7). We note that seven images were taken in the afternoon within a 30 min range, which makes them unsatisfying to measure significant dispersion on true North direction. The two images selected here are corresponding to the maximum deviation.

Each image is compared with a simulation and labeled with time in UTC, Local Mean Solar Time (LMST), Local True Solar Time (LTST), angles H (hour angle), α (right ascension), δ (declination), A (azimuth) and h (elevation) expressed in degrees and the simulated shadow length in millimeters.

3.6. Discussion

On the two images presented here, the True North direction is determined using the computed Sun azimuth (Figures 6 and 7). By using the gnomon shadow top, determined as precisely as possible given the shape of the instrument and images resolution, the North-South axis is graphically determined. The axis is drawn as a black line on both pictures. A difference of almost half a segment on the target is visible between the two pictures. Since a segment has a thickness of 5°, the deviation between the two images correspond to almost 2.5°.

One can notice that the first image is taken almost at noon. The true North direction determination is thus expected to be easier on that specific image. However, as discussed by Savoie et al. (2019), the error made on true North determination at noon is larger due to the rapid motion of the Sun, the equatorial position of the lander and the short shadow length. The image is thus suspected to be less accurate than the others.

These two images correspond to the maximum deviation we obtain on the eight images of January 1st. Based on those images, the True North direction on InSight landing site can be determined within a 2.5° range. Unfortunately, this result is over the expected 1° accuracy for an optimal Martian sundial use. This lack of accuracy can be explained by the very similar shadow positions induced by images taken on a very short time range. The accuracy of this measurement could have been increased by images taken through the whole day, morning and afternoon, as suggested by Savoie et al. (2019).

However, an accuracy of 2.5° on the True North direction is below the required accuracy of 5° of the SEIS instrument. The sundial experiment thus was able to meet its requirements.

4. Location of SEIS and Knowledge of North

The location of the InSight spacecraft on the surface of Mars has been determined in both inertial space by X-band radio tracking by the Rotation and Interior Structure Experiment (RISE) (Folkner et al., 2018) and by a high-resolution image acquired from orbit that clearly resolves the lander and the large circular solar panels that has been georeferenced to the cartographic grid (Golombek, Warner, et al., 2020). A 30 cm/pixel High-Resolution Imaging Science Experiment (HiRISE) image acquired on December 6, 2018 after landing has been carefully georeferenced to image and topographic basemap composed of 12.5 m/pixel High-Resolution Stereo Camera (HRSC) images, 6 m/pixel MRO Context Camera (CTX) images in the International Astronomical Union/International Association of Geodesy, IAU/IAG 2000 positive East planetocentric coordinate system with 463 m/pixel Mars Orbiter Laser Altimeter (MOLA) elevation postings as its base. In this system, the center of the lander is located at 4.50,238,417°N, 135.62,344,690°E, at an elevation of −2,613.426 m (Golombek, Warner, et al., 2020).

After placing SEIS in the workspace to the south of the lander, several methods were used to determine its location (Golombek, Williams, et al., 2020). Stereo IDC images of the instruments and their fiducial points

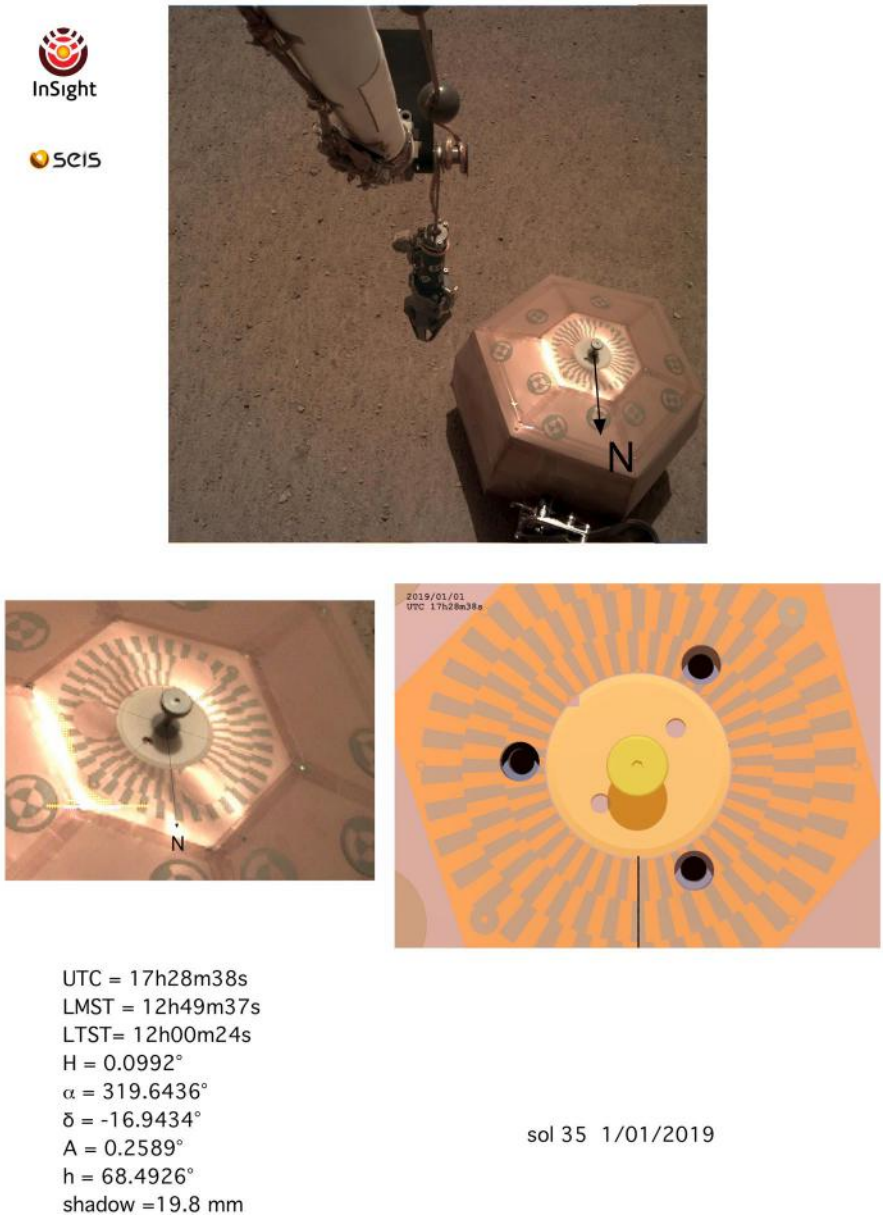

Figure 6. True North direction for image taken on Sol 35 (1-1-2019), 17h28m38s UTC.

were used as was the physical location of the arm by moving the grapple (used to pick up the instruments) directly above SEIS. These determinations were made in spacecraft centered coordinate systems. IDC stereo mosaics were also tied to the HiRISE image by transforming the spacecraft coordinate systems into the cartographic frame (Golombek, Williams, et al., 2020). These different methods locate the grapple/hook point of SEIS at 4.50,234,460°N, 135.62,343,703°E with its feet at an elevation of − 2,613.4 m with respect to the MOLA geoid.

The transformation of lander coordinates to Mars (the site frame) includes knowledge of the spacecraft yaw, pitch and roll recorded by the spacecraft Inertial Measurement Unit (IMU, Golombek, Williams, et al., 2020). To test if there are any errors in our knowledge of the orientation of the spacecraft, the azimuths of features that are in view in both the surface panoramas and the HiRISE image were compared. The azimuths of around 35 features matches to within 1°. The best matched features greater than 50 m away, where discrepancies would be greatest, agree to an average of 0.5°. This suggests that the orientation

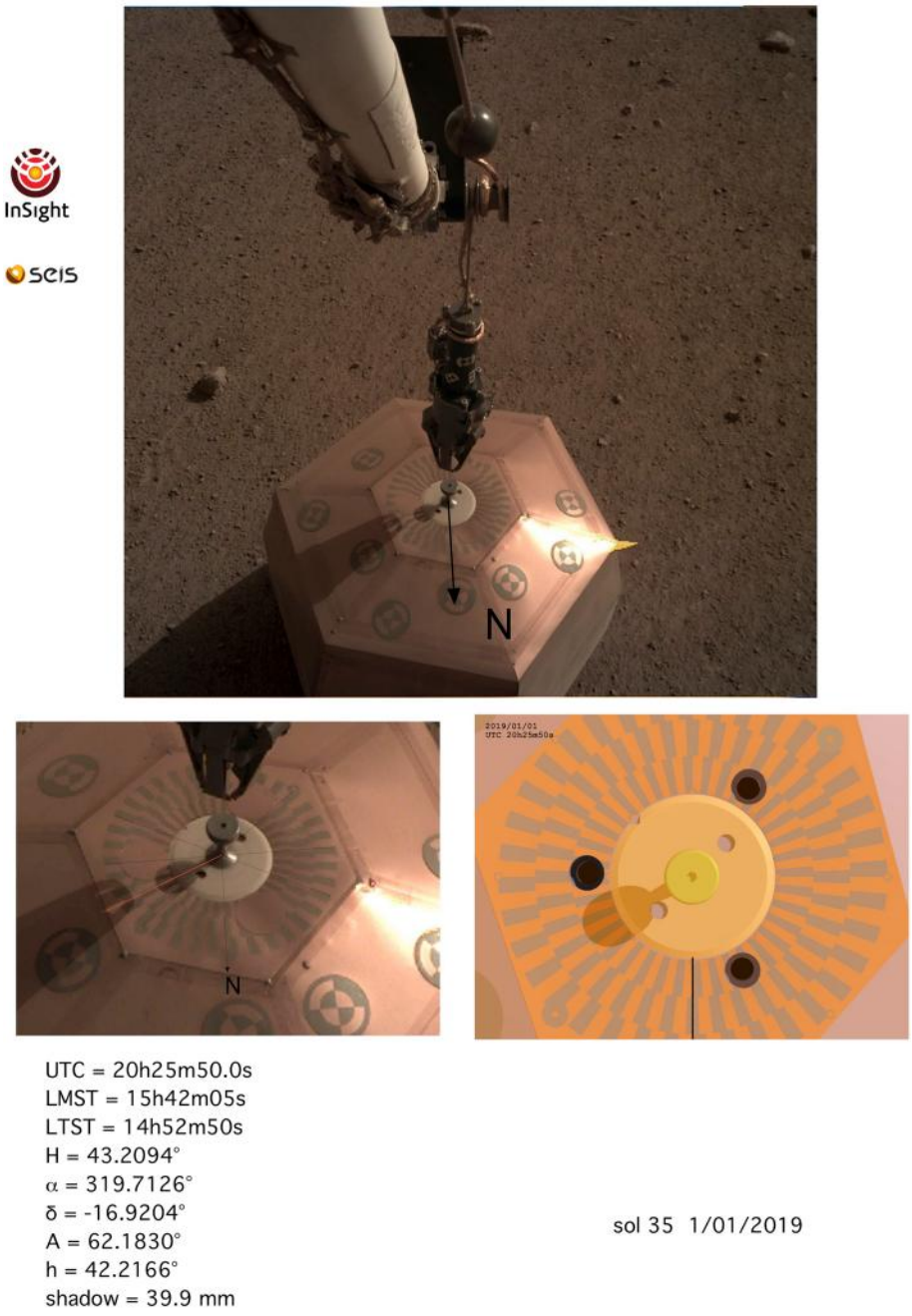

Figure 7. True North direction for image taken on Sol 35 (1-1-2019), 20h25m50s UTC.

(including the azimuth and tilt) recorded by the IMU and used to determine the site frame are accurate. This also means that analyses using lander images that depend on the location, azimuth and tilt of the spacecraft are accurate.

5. Comparison of the Gnomonic True North Direction with the Inertial Measurement Unit Value in SEIS Reference Frame

Independently from the gnomon experiment, orientation of the SEIS instrument has been measured by using the Inertial Measurement Unit (IMU). Golombek, Williams, et al. (2020) gives SEIS ground location expressed in the site frame. The site frame was determined by IMU measurement during descent, with Z

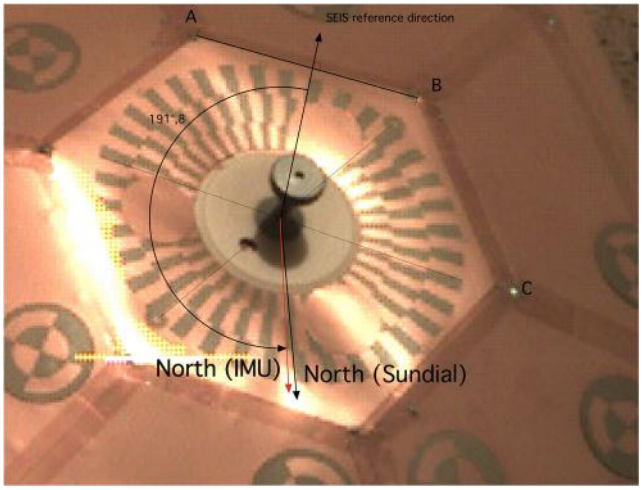

Figure 8. Comparison between sundial north determination and IMU north direction.

axis along the gravity vector, *X* north and *Y* east. Knowing SEIS center location, we define SEIS reference direction as the middle of one of its hexagonal borders (see Figure 8). Angles of the hexagon can be computed as reference points expressed in the site frame. Using these reference points leads to the reference direction azimuth expressed from true North direction.

The azimuth of SEIS reference direction expressed using the site frame coordinates is 191.8° (±1°) (Table 2).

This azimuth is in good agreement with the north direction obtained using the mean value of true North direction from the eight images of the gnomon as seen in Figure 8, with an error of about 2.5°.

6. Seismic Requirements and Seismic Errors in seismic Azimuth Determination

The Marsquake Service (Clinton et al., 2018, 2020) maintains a catalog of marsquakes (InSight Marsquake Service, 2020) that includes phase identification and location information, when possible. By March 2020, only three events have been detected that include clearly identifiable polarized motions for first P and S arriving phases (Giardini et al., 2020; Clinton et al., 2020). At longer periods, no Rayleigh surface waves have been detected in these three events nor in any other and could therefore not be used for location as originally proposed by Panning et al. (2015). Figure 9 shows vertical component seismograms and horizontal particle motions from the VBB sensor for these three events. The North and East directions in the horizontal particle motions have been computed by transforming the three axis VBBs into *Z* (Vertical downward), North and East components, by using for each of the VBB sensors their azimuth with respect to North, as a composition of the azimuth between North and the SEIS reference direction, as determined by the gnomon, and the azimuth of each axis with with that SEIS reference direction, determined prelaunch. The resulting azimuths are included in the SEIS dataless of all SEIS axis (InSight Mars SEIS Data Service, 2019).The P-picks are taken from InSight Marsquake Service (2020). The time windows selected for polarization analysis and the horizontal particle motion are indicated in the time series. The red line on the particle motion plots indicates the azimuth chosen visually, the shaded gray area indicates the estimated uncertainty. The 180° ambiguity can be resolved by considering the vertical component polarity as described by Böse et al. (2017). The raw seismograms were only multiplied by gain and filtered in the range indicated in Table 3. Azimuths are those proposed by Clinton et al. (2020) with errors determined by the 25% of the peak values. These errors estimated from MQS for these seismic events are larger than the differences in the mean azimuth found by different techniques. Lognonné et al. (2020) for example used, for the event S0173a, the polarization analysis of Schimmel et al. (2011) and found for the P an azimuth of 93° (larger by 3° as MQS estimate), while the azimuth of the S ranges from 163.1° to 181° in the 0.3–0.4 Hz and 0.4–0.7 Hz bandwidth respectively. While the high frequency S azimuth is found to be, as expected, almost orthogonal to the P one, the lower frequency illustrates the sensitivity of the techniques to both noise and, for the S wave, to the P seismic coda. In addition, lateral variation are expected to generate off-path perturbation of body waves as illustrated by several Earth studies (e.g. Otsuka, 1966), as well as off-great circle deviation of surface waves (Laske, 1995). From a seismological perspective, the ±2.5° error in the True North direction is therefore comparable to the differences found between different azimuth determination techniques and is also likely less than the expected effects of lateral variation on both body and surface waves ray azimuth.

Table 2
Values of Azimuth of the SEIS Reference Direction Expressed With IMU and the Gnomon

Instrument	SEIS reference direction azimuth
IMU	191.8° ± 1°
Gnomon	195° ± 2.5°

7. Conclusion

By using eight images taken during Sol 35 of the InSight surface activity, we were able to estimate the Sun direction and compute its local coordinates over the landing site. The results presented in this paper show that we were able to graphically determine the True North direction of

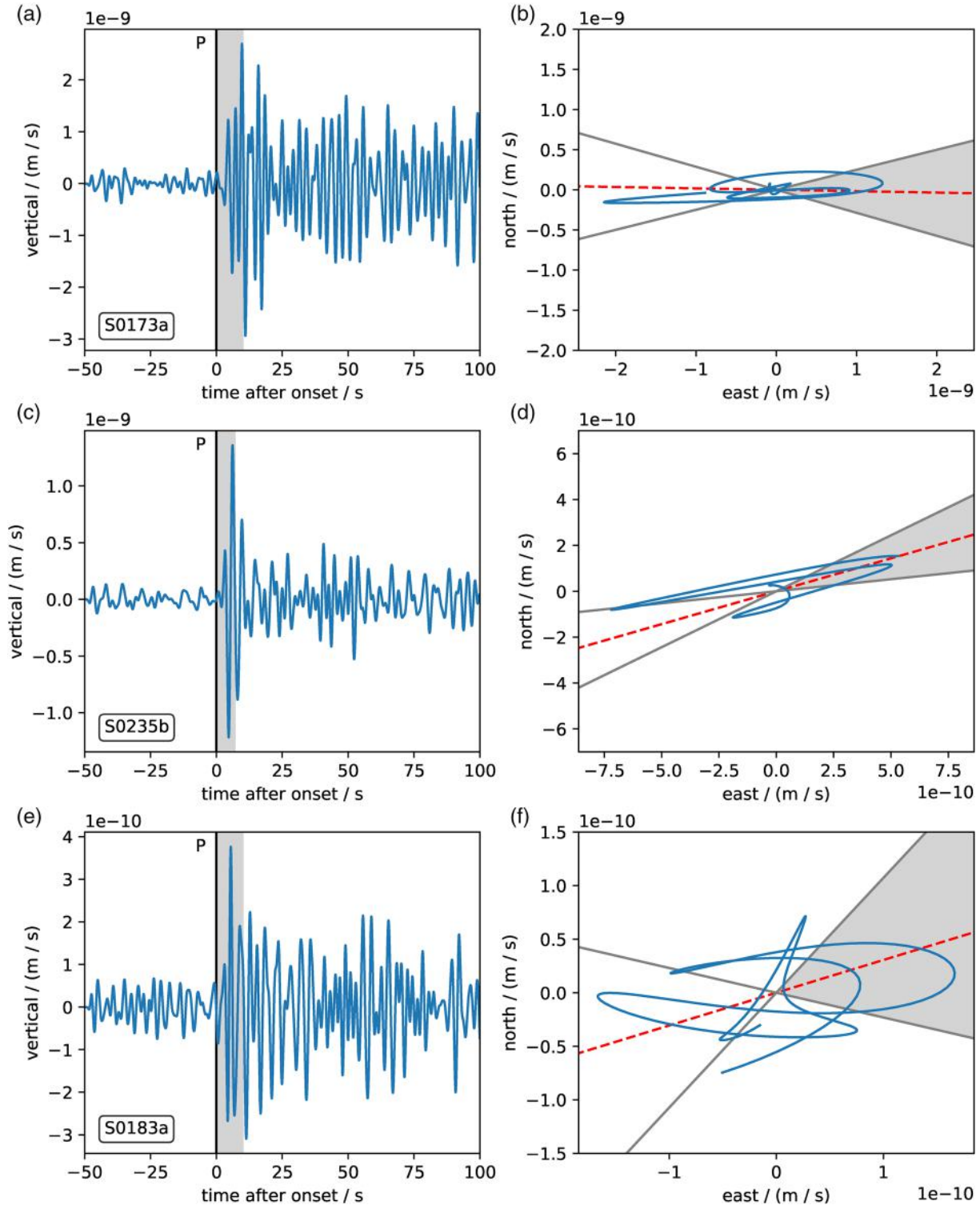

Figure 9. Vertical component VBB seismograms and horizontal particle motion for the three events with clearest polarization (S0173a, S0235b, S0183a). The red line on the particle motion plots indicates the azimuth chosen visually, the shaded gray area indicates the estimated uncertainty. Details on error determination methods are in Clinton et al. (2020).

Table 3
Processing Details for the Azimuth Determination of Mars Quakes in Figure 9 and Associated Azimuth and Errors, Following Clinton et al. (2020)

Event	Filter range/Hz	Window length/s	Azimuth	Error
S0173a	0.167–0.5	10	90°	− 11/+ 12°
S0235b	0.125–0.5	7	74°	− 8/+ 14°
S0183a	0.2–0.5	10	72°	− 11/+ 10°

the deployed seismometer at the landing site within a 2.5° range. This accuracy is below the requirement of 5° for the SEIS experiment, and well below the level of uncertainty that can be estimated for marsquakes observed to date. Comparison of the north direction obtained with the gnomon measurements is compatible with IMU north direction of the lander within 2.5°, suggesting the use of such a simple device as a sundial can continue to be used for orientation of instruments on space missions.

In conclusion, the sundial did fulfill its expectations. It is a success for the first sundial on another planet. Even though Curiosity and the MER rovers included a sundial device called MarsDial, it is important to notice that these are artistic devices used as calibration targets for cameras and pedagogic resources for scholars on Earth. They were not intended to provide any rigorous astronomical measurements. The SEIS sundial (which is rather a solar compass) is the first martian sundial successfully used for an astronomical purpose. This martian sundial experiment shows once again the possibilities of this ancient and passive tool for actual space missions.

Data Availability Statement

All imaging data used in this paper are freely available at the Planetary Data system (PDS) at https://pds-imaging.jpl.nasa.gov/data/nsyt/insight_cameras/, including timing. SEIS data. We acknowledge NASA, CNES, their partner agencies and Institutions (UKSA, SSO, DLR, JPL, IPGP-CNRS, ETHZ, IC, MPS-MPG) and the flight operations team at JPL, SISMOC, MSDS, IRIS-DMC and PDS for providing SEED SEIS data used in section 5 and freely available at IPGP MSDS, IRIS-DMC and PDS (https://doi.org/10.18715/SEIS.INSIGHT.XB_2016). The Marsquake Catalog, version 3 (https://doi.org/10.12686/a7) used in section 5 is available from IPGP and PDS.

The authors would like to thank Boris Semenov (JPL/NAIF Team) for its help on the time determination of SEIS images.

Acknowledgments
A portion of this work was supported by the InSight Project at the Jet Propulsion Laboratory, California Institute of Technology, under a contract with the National Aeronautics and Space Administration.
French co-authors acknowledge the support of CNES and of the Agence Nationale de la Recherche (ANR-14-CE36-0012-02 and ANR-19-CE31-0008-08).
This is InSight contribution number 175.

References

Bruce Banerdt, W., Smrekar, S. E., Banfield, D., Giardini, D., Golombek, M., Johnson, C. L., et al. (2020). Initial results from the InSight mission on Mars. *Nature Geoscience*, 1–7. https://doi.org/10.1038/s41561-020-0544-y

Böse, M., Clinton, J. F., Ceylan, S., Euchner, F., van Driel, M., Khan, A., et al. (2017). A probabilistic framework for single-station location of seismicity on Earth and Mars. *Physics of the Earth and Planetary Interiors*, *262*, 48–65. https://doi.org/10.1016/j.pepi.2016.11.003

Clinton, J., Giardini, D., Böse, M., Ceylan, S., van Driel, M., Euchner, F., et al. (2018). The marsquake service: Securing daily analysis of SEIS data and building the Martian seismicity catalog for InSight. *Space Science Reviews*, *214*(8). https://doi.org/10.1007/s11214-018-0567-5

Clinton, J. F., Ceylan, S., Martin van Driel, Giardini, D., Stähler, S. C., Böse, M., et al. (2020). The marsquake catalog from insight, sols 0–478. *Physics of the Earth and Planetary Interiors*. https://doi.org/10.1016/j.pepi.2020.10659

Folkner, W. M., Dehant, V., Le Maistre, S., Yseboodt, M., Rivoldini, A., Van Hoolst, T., et al. (2018). The rotation and interior structure experiment on the InSight mission to Mars. *Space Science Reviews*, *214*(5), 100. https://doi.org/10.1007/s11214-018-0530-5

Giardini, D., Lognonné, P., Banerdt, W. B., Pike, W. T., Christensen, U., Ceylan, S., et al. (2020). The seismicity of Mars. *Nature Geoscience*, *13*, 205–212. https://doi.org/10.1038/s41561-020-0539-8

Golombek, M., Warner, N. H., Grant, J. A., Hauber, E., Ansan, V., Weitz, C. M., et al. (2020). Geology of the InSight landing site on Mars. *Nature Communications*, *11*, 1014. https://doi.org/10.1038/s41467-020-14679-1

Golombek, M., Williams, N., Warner, N. H., Parker, T., Williams, M. G., Daubar, I., et al. (2020). Location and setting of the InSight lander, instruments and landing site. *Earth and Space Science*, *7*(10), e2020EA001248. https://doi.org/10.1029/2020EA001248

InSight Mars SEIS Data Service (2019). *Seis raw data, Insight mission*. IPGP, JPL, CNES, ETHZ, ICL, MPS, ISAE-Supaero, LPG, MFSC. https://doi.org/10.18715/SEIS.INSIGHT.XB_2016

InSight Marsquake Service (2020). *Mars seismic catalog, insight mission; v2 2020-04-01*. ETHZ, IPGP, JPL, ICL, ISAE-Supaero, MPS, Univ. Bristol. https://doi.org/10.12686/a7

Kuhnke, F., Menvielle, M., Musmann, G., Francois Karczewski, J., Kügler, H., Cavot, C., et al. (1998). The OPTIMISM/MAG mars-96 experiment: magnetic measurements onboard landers and related magnetic cleanliness program. *Planetary and Space Science*, *46*(6–7), 749–767. https://doi.org/10.1016/s0032-0633(98)00010-5

Laske, G. (1995). Global observation of off-great-circle propagation of Long-Period surface waves. *Geophysical Journal International*, *123*(1), 245–259. https://doi.org/10.1111/j.1365-246X.1995.tb06673.x

Linkin, V., Harri, A.-M., Lipatov, A., Belostotskaja, K., Derbunovich, B., Ekonomov, A., et al. (1998). A sophisticated lander for scientific exploration of mars: scientific objectives and implementation of the mars-96 small station. *Planetary and Space Science*, *46*(6–7), 717–737. https://doi.org/10.1016/s0032-0633(98)00008-7

Lognonné, P., Banerdt, W. B., Giardini, D., Pike, W. T., Christensen, U., Laudet, P., et al. (2019). SEIS: Insight's seismic experiment for internal structure of Mars. *Space Science Reviews*, *215*(1), 12. https://doi.org/10.1007/s11214-018-0574-6

Lognonné, P., Banerdt, W. B., Pike, W. T., Giardini, D., Christensen, U., Garcia, R. F., et al. (2020). Constraints on the shallow elastic and anelastic structure of Mars from InSight seismic data. *Nature Geoscience*, 213–220. https://doi.org/10.1038/s41561-020-0536-y

Lognonné, P., Zharkov, V. N., Karczewski, J. F., Romanowicz, B., Menvielle, M., Poupinet, G., et al. (1998). The seismic OPTIMISM experiment. *Planetary and Space Science*, *46*(6–7), 739–747. https://doi.org/10.1016/s0032-0633(98)00009-9

Maki, J. N., Golombek, M., Deen, R., Abarca, H., Sorice, C., Goodsall, T., et al. (2018). The color cameras on the InSight lander. *Space Science Reviews*, *214*(6), 105. https://doi.org/10.1007/s11214-018-0536-z

Otsuka, M. (1966). Azimuth and slowness anomalies of seismic waves measured on the central California seismographic array. Part I. Observations. *Bulletin of the Seismological Society of America*, *56*(1), 223–239.

Panning, M. P., Beucler, E., Drilleau, M., Mocquet, A., Lognonné, P., & Banerdt, W. B. (2015). Verifying single-station seismic approaches using Earth-based data: Preparation for data return from the InSight mission to Mars. *Icarus*, *248*, 230–242. https://doi.org/10.1016/j.icarus.2014.10.035

Parker, T. J., Golombek, M. P., Calef, F. J., Williams, N. R., LeMaistre, S., Folkner, W., et al. (2019). Localization of the InSight lander. In *Lunar and Planetary Science Conference, Lunar and Planetary Science Conference*, 1948. Retrieved from https://www.ncbi.nlm.nih.gov/pmc/articles/PMC7583488/

Savoie, D., Richard, A., Goutaudier, M., Onufer, N. P., Wallace, M. C., Mimoun, D., et al. (2019). Determining true north on Mars by using a sundial on InSight. *Space Science Reviews*, *215*(2). https://doi.org/10.1007/s11214-018-0568-4

Schimmel, M., Stutzmann, E., Ardhuin, F., & Gallart, J. (2011). Polarized Earth's ambient microseismic noise. *Geochemistry, Geophysics, Geosystems*, *12*(7). Q07014. https://doi.org/10.1029/2011GC003661

Sullivan, T. A. (1994). *Catalog of Apollo experiment operations*. USRA Houstan Repository. Retrieved from https://www.hq.nasa.gov/alsj/RP-1994-1317.pdf